Macrophages facilitate electrical conduction in the heart

Maarten Hulsmans[1]†, Sebastian Clauss[2,3,4]†, Ling Xiao[2]†, Aaron D. Aguirre[1,2], Kevin R. King[1], Alan Hanley[2], William J. Hucker[2], Eike M. Wülfers[5,6], Gunnar Seemann[5,6], Gabriel Courties[1], Yoshiko Iwamoto[1], Yuan Sun[1], Hendrik B. Sager[1], Kory J. Lavine[7], Gregory A. Fishbein[8], Diane E. Capen[1], Nicolas Da Silva[1], Lucile Miquerol[9], Kamila Naxerova[10], Richard N. Mitchell[8], Dennis Brown[1], Peter Libby[11], Ralph Weissleder[1,12], Filip K. Swirski[1], Peter Kohl[5,6,13], Claudio Vinegoni[1], David J. Milan[2,14], Patrick T. Ellinor[2,14] & Matthias Nahrendorf[1,2,*]

Affiliations:

[1]Center for Systems Biology, Massachusetts General Hospital, Harvard Medical School, Boston, Massachusetts 02114, USA.

[2]Cardiovascular Research Center, Massachusetts General Hospital, Harvard Medical School, Boston, Massachusetts 02114, USA.

[3]Department of Medicine I, Klinikum Grosshadern, University of Munich, 81377 Munich, Germany.

[4]German Center for Cardiovascular Research, Partner site Munich, Munich Heart Alliance, Germany.

[5]Institute for Experimental Cardiovascular Medicine, University Heart Centre Freiburg, Bad Krozingen, 79110 Freiburg, Germany.

[6]Faculty of Medicine, Albert-Ludwigs University, 79110 Freiburg, Germany.

[7]Center for Cardiovascular Research, Washington University School of Medicine, St. Louis, Missouri 63110, USA.

[8]Department of Pathology, Brigham and Women's Hospital, Harvard Medical School, Boston, Massachusetts 02115, USA.

[9]Aix Marseille Univ, CNRS, IBDM, Marseille, France.

[10]Department of Genetics, Brigham and Women's Hospital, Harvard Medical School, Boston, Massachusetts 02115, USA.

[11]Cardiovascular Division, Department of Medicine, Brigham and Women's Hospital, Harvard Medical School, Boston, Massachusetts 02115, USA.

[12]Department of Systems Biology, Harvard Medical School, Boston, Massachusetts 02115, USA.

[13]Cardiac Biophysics and Systems Biology, National Heart and Lung Institute, Imperial College London, London SW36NP, UK.

[14]Program in Population and Medical Genetics, The Broad Institute of Harvard and MIT, Cambridge, Massachusetts 02142, USA.

†These authors contributed equally to this work.

37 **SUMMARY**

38 Organ-specific functions of tissue-resident macrophages in the steady-state heart are unknown.

39 Here we describe that cardiac macrophages facilitate electrical conduction through the distal

40 atrioventricular node, where conducting cells densely intersperse with elongated macrophages

41 expressing connexin 43. When coupled to spontaneously beating cardiomyocytes via connexin

42 43-containing gap junctions, cardiac macrophages have a negative resting membrane potential

43 and depolarize in synchrony with cardiomyocytes. Conversely, macrophages render the resting

44 membrane potential of cardiomyocytes more positive and, according to computational modeling,

45 accelerate their repolarization. Photostimulation of channelrhodopsin 2-expressing macrophages

46 improves atrioventricular conduction, while conditional deletion of connexin 43 in macrophages

47 and congenital lack of macrophages delay atrioventricular conduction. In the $Cd11b^{DTR}$ mouse,

48 macrophage ablation induces progressive atrioventricular block. These observations implicate

49 macrophages in normal and aberrant cardiac conduction.

50

INTRODUCTION

Studies in the late 19th century first described macrophages as phagocytic cells that defend the organism against pathogens[1]. More recently, it became clear that resident macrophages populate all tissues and pursue organ-specific functions. For instance, macrophages contribute to thermogenesis regulation in adipose tissue[2], iron recycling in the spleen and liver[3] and synaptic pruning in the brain[4]. These non-canonical activities highlight macrophages' functional diversity and emphasize their ability to execute tissue-specific tasks beyond host defense[5].

The cardiac conduction system coordinates the heart's electrical activation. Electrical impulse generation begins in the sinoatrial node and sequentially propagates activation of the atria, atrioventricular (AV) node, His and Purkinje systems, and ventricles. By providing the only electrical connection between the atria and ventricles, the AV node plays an essential role. First described by Tawara in 1906[6], the AV node is located at the base of the right atrium and contains cardiomyocytes with a distinct action potential[7]. Clinically, AV block delays or abolishes atrial impulse conduction to the ventricles, which can lead to hemodynamic deterioration, syncope and death if not treated with pacemaker implantation[8].

Macrophages are an intrinsic part of the healthy working myocardium, where they appear as spindle-like cells interspersed among myocytes, fibroblasts and endothelial cells[9–11]. Cardiac healing after injury requires macrophages[12]; however, in contrast to other organs, specific functions of cardiac macrophages in the steady-state are unknown. Here we report resident macrophages' abundance in the distal AV node and show that they contribute to cardiac conduction.

Macrophages abound in the AV node

Resident macrophages are present in the left ventricle (LV), but prior work did not report on intra-organ heterogeneity. It therefore remained unclear whether macrophages distribute homogeneously throughout the heart and whether any reside in the conduction system. To investigate macrophages' presence and spatial distribution in the intact AV node, we optically cleared and imaged entire AV nodes of $Cx_3cr1^{GFP/+}$ mice, in which fluorescent protein identifies macrophages, by confocal microscopy (Fig. 1a). We found that HCN4-expressing cardiomyocytes[13], in particular in the lower nodal or AV bundle, frequently intersperse with macrophages (Fig. 1b). AV node macrophages assume an elongated, spindle-shaped appearance with far-reaching cytoplasmic projections (Fig. 1c). To study the morphological characteristics of AV node macrophages by electron microscopy, we labeled GFP$^+$ macrophages in $Cx_3cr1^{GFP/+}$ mice with diaminobenzidine (DAB). DAB$^+$ macrophages display long cellular processes that closely associate with cardiomyocytes (Fig. 1d).

To compare macrophage numbers in the AV node with the LV myocardium, we investigated microdissected tissue by flow cytometry. The mouse AV node has a higher macrophage density than the LV (Fig. 2a). Similar to mice, CD68$^+$ macrophages were more abundant in human AV nodes than in working myocardium (Extended Data Fig. 1a, b). In the mouse AV node, the majority of the CD45$^+$ leukocytes are CD11b$^+$ F4/80$^+$ Ly6C^{low} macrophages. The expression of CD64 and CX$_3$CR1 and the lack of CD11c and CD103 confirm that these cells are macrophages and not dendritic cells (Fig. 2b). Steady-state myocardial tissue-resident macrophages primarily arise from embryonic yolk-sac progenitors and perpetuate independently of monocytes through *in situ* proliferation[10,11]. Using parabiosis, we determined that circulating cells contributed minimally to AV node macrophages, similar to LV free wall macrophages (Fig. 2c).

96   Single-cell RNA-sequencing (RNA-seq) of AV node macrophages showed cellular subsets that

97   are also present elsewhere in the heart[11] (Fig. 2d). These macrophage subsets separated based on

98   their expression of major histocompatibility complex class II (*H2*) and chemokine receptor 2

99   (*Ccr2*) (Extended Data Fig. 2a-c). RNA-seq and quantitative real-time PCR (qPCR) revealed that

100   AV node macrophages express ion channels and exchangers (Extended Data Fig. 2d, e), while

101   deposited microarray data[9] show cardiac macrophages' enrichment of genes associated with

102   conduction (Extended Data Fig. 2f).

103   **Connexin 43 connects macrophages with myocytes**

104   Gap junctions, which are formed by connexin (Cx) proteins, connect two adjacent cells'

105   cytoplasm and enable intercellular communication[14]. Most tissues as well as immune cells

106   express Cx43[15]. Cx43-containing gap junctions electrically couple cardiomyocytes, enable

107   electrical impulse propagation, and consequently coordinate synchronous heart muscle

108   contractions[16]. In addition, Cx43-containing gap junctions couple cardiomyocytes with non-

109   cardiomyocytes, which can thereby alter the electrophysiological properties of cardiomyocytes[17].

110   To determine if AV node macrophages express proteins that give rise to gap junctions, we

111   evaluated six connexins found in leukocytes[18] in FACS-purified cells harvested from

112   microdissected AV nodes. AV node macrophages mainly express *Cx43* (Fig. 3a). We next sorted

113   macrophages from the peritoneal cavity and compared their *Cx43* levels with AV node

114   macrophages and whole AV node tissue. AV node macrophages express *Cx43* at much higher

115   levels than peritoneal macrophages (Fig. 3b). To ensure the purity of sorted macrophage

116   populations, we measured different macrophage-[19] and cardiomyocyte-specific markers[20] in

117   FACS-purified macrophage populations. All macrophage samples display a characteristic

118   macrophage signature (Extended Data Fig. 3a) and lack expression of cardiomyocyte-specific

119   genes (Extended Data Fig. 3b). As reported previously, peritoneal macrophages express *Gata6*[21]

120   but AV node macrophages do not (Extended Data Fig. 3b).

121   We then analyzed the Cx43 protein expression in AV node macrophages by whole-mount

122   immunofluorescence in the lower AV node, an area in which conducting cells express this

123   connexin[22,23]. Cx43 marks contact points between CX_3CR1^+ macrophages and $HCN4^+$

124   cardiomyocytes, suggesting gap junction-mediated intercellular communication between both

125   cell types in the distal AV node (Fig. 3c). Electron microscopy also visualized contact sites

126   between AV node macrophages and conducting cardiomyocytes (Fig. 3d). Functional gap

127   junction connections between macrophages and conducting cardiomyocytes were suggested by

128   rapid distribution of the gap junction-permeable dye Lucifer yellow in an *ex vivo* scrape-loading

129   and dye transfer assay. Spread of Lucifer yellow in conducting cardiomyocytes and transfer to

130   neighboring CX_3CR1^+ macrophages occurred within 10 minutes (Extended Data Fig. 3c).

131   Together, these observations establish the presence of functional gap junctions between

132   conducting cells and AV node macrophages.

133   **Macrophages electrically modulate myocytes**

134   Since gap junctions electrotonically couple neighboring cells[24], we next tested the hypothesis

135   that macrophages enter electrotonic communication with adjacent cardiomyocytes. We began by

136   investigating the membrane potential of FACS-purified cardiac macrophages attached to

137   neonatal mouse cardiomyocytes using whole-cell patch clamp. As observed *in vivo*, Cx43

138   localized at sites of macrophage-cardiomyocyte interaction, indicating gap junction

139   communication between these cell types in culture (Fig. 3e). $TexasRed^+$ dextran entering GFP^+

140 macrophages from the micropipette (Fig. 3f) confirms that our membrane potential recording

141 derived from macrophages. Spontaneously-beating cardiomyocytes displayed a typical resting

142 membrane and action potential[25] (Fig. 3g). The resting membrane potential in solitary cardiac

143 macrophages is depolarized relative to that of cardiomyocytes (Fig. 3g). We documented values

144 between -35 and -3 mV that correspond well with data reported for human monocyte-derived and

145 mouse peritoneal macrophages[26,27] (Fig. 3h). There was no spontaneous depolarization in solitary

146 cardiac macrophages (Fig. 3g). We next recorded the membrane potential in cardiac

147 macrophages attached to beating cardiomyocytes. 23% of these macrophages rhythmically

148 depolarized with a distinct action potential morphology, characterized by a slowed upstroke and

149 reduced maximal polarization when compared to the isolated cardiomyocyte (Fig. 3g). These

150 cardiomyocyte-linked macrophages' resting membrane potentials were more negative than those

151 of solitary macrophages, indicating electrical coupling (Fig. 3h). We recorded irregular

152 depolarization in another 23% and lack of activity in the remaining 54% (Extended Data Fig.

153 4a). Macrophages with any kind of depolarization, either regular or irregular, had a more

154 negative resting membrane potential than non-depolarizing macrophages (Extended Data Fig.

155 4b). To simultaneously record action potential-related fluorescence changes in macrophages and

156 cardiomyocytes, we examined cardiomyocyte-driven macrophage depolarization using the

157 ANNINE-6plus voltage-sensitive dye. These data show that macrophage action potentials are

158 synchronous with action potentials of cardiomyocytes (Extended Data Fig. 4c, d).

159 Next we investigated whether macrophages change the electrical properties of coupled

160 cardiomyocytes. Indeed, macrophages render cardiomyocyte resting membrane potentials more

161 positive, an effect that was reversed by pharmacological Cx43 blockade (Fig. 3i). Inhibition of

162 Cx43-mediated gap junctions in solitary cardiomyocytes did not change their resting membrane

163 potential (Extended Data Fig. 4e).

164 To explore the consequences of the observed communication between macrophages and

165 cardiomyocytes, we pursued mathematical modeling of electrical interactions between

166 macrophages and AV cardiomyocytes (see Supplementary Table 1 for model parameters).

167 Recapitulating the experimental data (Fig. 3i), modeling indicates that the cardiomyocyte resting

168 membrane potential is more depolarized when the cell is coupled to a macrophage, an effect that

169 increases with gap junction conductance (Extended Data Fig. 4f). Modeling suggests that

170 coupling increasing numbers of macrophages accelerates cardiomyocyte repolarization (Fig. 3j).

171 For example, coupling three macrophages to an AV bundle cardiomyocyte, a ratio supported by

172 histology (3 ± 0.3, mean $\pm$ s.e.m., $n = 17$ in 5 mice; Fig. 1 and Fig. 3c), decreases cardiomyocyte

173 action potential duration from 30 ms to 21 ms while depolarizing the resting membrane potential

174 from -69 mV to -52 mV (Fig. 3k, l), assuming a gap junction conductance of 1 nS. *In vivo*, a

175 shorter action potential duration would decrease the effective refractory period of the myocyte

176 and increase the frequency at which it can be depolarized. A higher resting membrane potential

177 would facilitate depolarization with less stimulation. Both alterations facilitate AV conduction at

178 higher frequencies. These results correspond well with prior conceptual models of electrotonic

179 interactions between cardiomyocytes and other electrically non-excitable cells[28].

180 To investigate cell-cell communication directly in the AV node, we expressed the

181 photoactivatable channelrhodopsin 2 (ChR2)[29] in macrophages to control their membrane

182 potential. When illuminated, the cation channel ChR2 undergoes a conformational change,

183 resulting in an immediate increase in ionic permeability with high conductance for Na^+ (ref. 30).

184 We posited that light-triggered cation influx into macrophages and their resulting depolarization

185 should alter AV node conduction if the cells are electrotonically coupled to conducting

186 cardiomyocytes. To this end, we bred tamoxifen-inducible Cx_3cr1^{CreER} with $ChR2^{fl/fl}$ mice to

187 obtain mice in which tamoxifen treatment triggers ChR2 expression in macrophages, hereafter

188 denoted $Cx_3cr1\ ChR2$. First, we validated macrophage-specific expression of the tamoxifen-

189 inducible Cre recombinase fusion protein (CreER) by measuring YFP fluorescence in heart

190 tissue, as YFP is co-expressed with CreER. We found that YFP signal colocalizes with CX_3CR1^+

191 macrophages whereas cardiomyocytes are YFP negative (Extended Data Fig. 5a). In addition,

192 after tamoxifen treatment, AV node macrophages specifically expressed the ChR2 protein, which

193 is fused with YFP (Extended Data Fig. 5b). We then retrogradely perfused hearts isolated from

194 $Cx_3cr1\ ChR2$ mice and inserted a fiber optic cannula into the right atrium to directly illuminate

195 the AV node region (please see Fig. 4a and Extended Data Fig. 5c for experimental setup). AV

196 node conduction was assessed by ECG during rapid electrical atrial pacing, comparing

197 continuous 470-nm wavelength illumination with no illumination. We observed improved AV

198 node conduction during photostimulation of macrophages in hearts harvested from $Cx_3cr1\ ChR2$

199 mice. Specifically, the Wenckebach ratio increased when the light was switched on, i.e. the

200 number of conducted atrial stimuli between two non-conducted impulses rose (Fig. 4b-d). In

201 $Cx_3cr1^{wt/CreER}$ control hearts, we observed no difference between illuminated and non-illuminated

202 states. Thus, opening the cation channel ChR2 in macrophages facilitates AV node conduction

203 during rapid pacing. Modeling indicates that with ChR2-induced tonic depolarization of

204 macrophages, the minimum heterocellular coupling required to achieve macrophage-mediated

205 passive action potential conduction between otherwise not connected cardiomyocytes becomes

206 smaller (Extended Data Fig. 6a, b). Taken together, our observations suggest that cardiac

207 macrophages can electrically couple to cardiomyocytes via gap junctions containing Cx43. This

208   leads to cyclical macrophage depolarization, modulates cardiomyocytes' electrophysiological

209   properties and alters AV nodal conduction.

Deleting Cx43 in macrophages delays AV conduction

210

211   The experiments described above indicate that macrophages present in the AV node may

212   facilitate conduction. To test this hypothesis in loss-of-function experiments, and to directly

213   investigate the importance of Cx43 in macrophages, we bred mice in which tamoxifen treatment

214   deleted Cx43 in CX$_3$CR1-expressing macrophages, hereafter denoted *Cx$_3$cr1 Cx43$^{-/-}$*. All mice

215   underwent analysis seven days after tamoxifen treatment (Fig. 5a). Genomic PCR-based

216   examination of the wild-type (*Cx43^{wt}*), floxed intact (*Cx43^{fl}*) and recombined (*Cx43$^{\Delta}$*) alleles of

217   the *Cx43* gene in FACS-purified CX$_3$CR1$^+$ cardiac macrophages showed effective *Cx43* deletion

218   in cardiac macrophages after tamoxifen treatment (Extended Data Fig. 7a). mRNA analysis

219   supported these findings (Extended Data Fig. 7b). Furthermore, the overall myocardial Cx43

220   protein level did not change, indicating unaltered Cx43 expression in other cardiac cells

221   (Extended Data Fig. 7c).

222   To determine how macrophage-specific Cx43 deletion affects AV nodal function, we performed

223   an *in vivo* electrophysiological (EP) study on *Cx$_3$cr1 Cx43$^{-/-}$* mice and littermate controls. The

224   AV node effective refractory period was prolonged in *Cx$_3$cr1 Cx43$^{-/-}$* mice (Fig. 5b). We

225   examined three additional parameters of AV nodal function including the pacing cycle lengths at

226   which Wenckebach conduction, 2:1 conduction and ventriculo-atrial Wenckebach conduction

227   occur. In *Cx$_3$cr1 Cx43$^{-/-}$* mice, each of these parameters was prolonged, indicating impaired AV

228   conduction (Fig. 5b). Representative surface ECG tracings of an AV Wenckebach block in

229   control and *Cx$_3$cr1 Cx43$^{-/-}$* mice are shown in Fig. 5c. There is progressive PR prolongation prior

230   to AV block, which develops at a slower pacing rate in *Cx₃cr1 Cx43⁻/⁻* mice compared to

231   controls. We did not observe differences in sinus node function or atrial refractory period

232   (Extended Data Table 1), and compromised AV conduction in *Cx₃cr1 Cx43⁻/⁻* mice was not

233   accompanied by altered AV node macrophage numbers (Fig. 5d, e). These data indicate that

234   macrophage Cx43 facilitates AV node conduction.

235   To explore the effect of congenital macrophage loss on AV node conduction, we performed an

236   EP study in *Csf1ᵒᵖ* mice, which lack Csf1-dependent tissue macrophages in many organs[31]. The

237   absence of AV node macrophages in *Csf1ᵒᵖ* mice (Fig. 5f, g) prolonged the AV node effective

238   refractory period as well as the pacing cycle lengths at which Wenckebach conduction and 2:1

239   conduction occurred (Fig. 5h). Interestingly, we also observed an increase in the atrial refractory

240   period of *Csf1ᵒᵖ* mice (Extended Data Table 1).

241   **Macrophage ablation induces AV block**

242   *Cd11bᴰᵀᴿ* mice express a diphtheria toxin (DT)-inducible system controlled by the human

243   *CD11b* promoter that enables efficient depletion of myeloid cells, including resident cardiac

244   macrophages[10]. We monitored these mice continuously by implantable ECG telemetry after

245   macrophage ablation (Fig. 6a). Maximum depletion of AV node macrophages happened three

246   days after a single dose of 25 ng/g body weight DT[10] (Fig. 6b). Within one day of DT injection,

247   all mice developed first degree AV block (Fig. 6c) that progressively evolved into second and

248   third degree AV block (Fig. 6d). Complete AV block coincided with the time point of peak AV

249   node macrophage depletion.

250   To determine whether the observed phenotype resulted from DT-related toxicity, we injected

251   C57BL/6 mice with DT and monitored their surface ECG. DT did not alter the number of AV

252 node macrophages in C57BL/6 mice (Fig. 6b) and did not induce AV block (Fig. 6c). At the time

253 of complete AV block, we did not observe increased cell death in AV nodes of $Cd11b^{DTR}$ mice

254 (Extended Data Fig. 8a). Because blood electrolyte levels may influence conduction, we

255 measured serum potassium and magnesium levels, which were unchanged (Extended Data Fig.

256 8b). Moreover, DT did not induce AV block in $Cx_3cr1^{GFP/+}$ mice joined in parabiosis with

257 $Cd11b^{DTR}$ mice, which developed AV block while in parabiosis, thereby indicating that

258 circulating factors do not contribute to the observed phenotype (Extended Data Fig. 8c).

259 Injections of isoproterenol, epinephrine and atropine did not attenuate the AV block (Extended

260 Data Fig. 8d). This suggests that the AV block induced by macrophage ablation did not result

261 from imbalanced autonomic nervous control.

262 Three loss-of-function experiments indicate that macrophages facilitate AV node conduction;

263 however, the observed phenotypes differ in their severity. To better understand the observed

264 differences, we compared the whole transcriptome of AV node tissue microdissected from

265 control, $Cx_3cr1\ Cx43^{-/-}$ and macrophage-depleted $Cd11b^{DTR}$ hearts by RNA-seq. The

266 transcriptional profile of $Cx_3cr1\ Cx43^{-/-}$ AV nodes resembled control nodal tissue with only four

267 genes significantly dysregulated while macrophage depletion led to a distinct expression profile

268 characterized by 1,329 differentially expressed genes (FDR < 0.05; Extended Data Fig. 8e and

269 Supplementary Tables 2, 3). Genes associated with cardiac conduction are expressed at lower

270 levels in macrophage-depleted AV nodes than in controls (Extended Data Fig. 8f). Thus, deletion

271 of Cx43 in macrophages had mild effects, while depletion of the cells changed the AV node

272 expression profile, and consequently its function, more drastically. These data suggest that AV

273 node macrophages engage in additional, Cx43 independent tasks, which may or may not be

274 related to conduction.

DISCUSSION

The presence of numerous resident macrophages in the normal myocardium has only recently gained recognition, a development aided by flow cytometry staining of cell surface marker combinations in tissue and macrophage-specific expression of fluorescent proteins[9–11]. We here employed optical clearing in combination with cell-specific reporter gene expression in macrophages to image their presence in whole AV nodes, documenting intra-organ macrophage heterogeneity. Moreover, we show that macrophages couple electrically to cardiomyocytes in the distal AV node via Cx43-containing gap junctions. The presence of Cx43-containing gap junctions in AV node tissue has previously been reported in humans and rabbits[23,32]. Cx43 shows relatively little expression within the compact node, but is observed in the lower nodal bundle. This Cx43-expressing region of the distal AV node contains a particularly dense macrophage population.

Cardiomyocytes electrotonically drive rhythmic depolarizations in coupled macrophages, which in turn alters the electrophysiological properties of coupled cardiomyocytes. Macrophages' electrotonic load depolarizes resting cardiomyocytes, reduces their action potential overshoot, and aids early repolarization which, according to computational modeling, shortens the cardiomyocyte action potential, ultimately allowing for higher rates of conducted beats. While depolarization of the resting membrane potential in working cardiomyocytes impairs excitation and conduction due to sodium channel inactivation, depolarization of AV nodal cells depends chiefly on calcium channels whose voltage-dependent inactivation is less prominent[33]. In addition, passive conduction via macrophages, as described for other non-myocytes[28], may pass on excitatory stimuli between AV node myocytes that are not in direct electrical contact. Taken together, these effects could increase the safety of AV node conduction. In support of this

298   concept, optogenetics depolarization of AV node macrophages improves AV conduction.

299   Impaired AV node conduction after i) macrophage-specific depletion of Cx43, ii) congenital lack

300   of macrophages and iii) acute depletion of macrophages adds further evidence that these cells

301   can facilitate nodal conduction (summary diagram, Extended Data Fig. 9).

302   Clinically, AV block is a common indication for pacemaker implantation, yet up to 60% of AV

303   block cases occur for unknown reasons[34]. Macrophages change in phenotype and number in

304   response to myocardial infarction[12] and heart failure[35], conditions associated with sudden cardiac

305   death as a result of ventricular arrhythmias[36]. Other inflammatory diseases of the heart, including

306   Chagas, Lyme, sarcoid and myocarditis cause conduction abnormalities. It will be important to

307   determine if these conditions produce AV block solely by affecting cardiomyocytes and

308   specialized conducting tissues as commonly assumed, or if cardiac macrophages, which rapidly

309   adapt their phenotype to inflammatory environments, are involved. Understanding macrophages'

310   contributions to normal cardiac conduction and to abnormalities in heart rhythm may yield new

311   pathophysiologic insight and suggest novel therapeutic strategies that could obviate the expense

312   and complications associated with the three million pacemakers currently implanted worldwide.

313

METHODS

Humans

Human AV node and LV tissues were obtained from fully de-identified heart specimens collected during routine autopsy of patients with no known cardiac conduction disease. Tissue sampling was approved by the Partners Healthcare Institutional Review Board under protocol #2015P001827.

Mice

C57BL/6 (stock 000664), B6.129P-$Cx3cr1^{tm1Litt}$/J (Cx_3cr1^{GFP}, stock 005582), B6.129P2(Cg)-$Cx3cr1^{tm2.1(cre/ERT)Litt}$/WganJ ($Cx_3cr1^{CreER}$, stock 021160), B6.Cg-$Gt(ROSA)26Sor^{tm32(CAG-COP4*H134R/EYFP)Hze}$/J ($ChR2^{fl/fl}$, stock 024109), B6.129S7-$Gja1^{tm1Dlg}$/J ($Cx43^{fl/fl}$, stock 008039), B6;C3Fe a/a-$Csf1^{op}$/J ($Csf1^{op/+}$, stock 000231), C57BL/6-Tg(UBC-GFP)30Scha/J (Ubc^{GFP}, stock 004353) and B6.FVB-Tg(ITGAM-DTR/EGFP)34Lan/J ($Cd11b^{DTR}$, stock 006000) were purchased from Jackson Laboratory. Genotyping for each strain was performed as described on the Jackson Laboratory website. One- to 2-day-old C57BL/6 pups (stock 027) were purchased from Charles River Laboratories. All experiments (except the isolation of neonatal mouse cardiomyocytes) were performed with 8- to 40-week-old animals and were carried out using age and gender matched groups. All mice were maintained in a pathogen-free environment of the Massachusetts General Hospital animal facility, and all animal experiments were approved by the Subcommittee on Animal Research Care at Massachusetts General Hospital.

334 *In vivo* **interventions**

335 Mice were put into parabiosis using either C57BL/6 and $Cx_3cr1^{GFP/+}$ or $Cd11b^{DTR}$ and

336 $Cx_3cr1^{GFP/+}$ mice as described previously[10]. Tamoxifen (Sigma) was given as a solution in corn

337 oil (Sigma) to $Cx_3cr1^{wt/CreER}$ $ChR2^{wt/fl}$ or $Cx_3cr1^{wt/CreER}$ $Cx43^{fl/fl}$ mice by intraperitoneal injection.

338 Animals received 5 doses of 2 mg of tamoxifen with a separation of 24 hours between doses.

339 $Cx_3cr1^{wt/CreER}$ $ChR2^{wt/fl}$ and $Cx_3cr1^{wt/CreER}$ $Cx43^{fl/fl}$ mice were analyzed 2 and 7 days post-

340 tamoxifen treatment, respectively. Macrophage depletion was achieved by a single

341 intraperitoneal injection of diphtheria toxin (DT, 25 ng/g body weight, Sigma) in $Cd11b^{DTR}$

342 mice[10]. C57BL/6 mice injected with DT were used as controls.

343 **EP study**

344 EP studies were performed under general anaesthesia induced by administering 5% isoflurane

345 driven by an oxygen source into an induction chamber. Anaesthesia was subsequently

346 maintained with 1-2% isoflurane in 95% O_2. For EP study, an octapolar catheter (Millar

347 Instruments) was inserted into the right jugular vein and positioned in the right atrium and

348 ventricle. Programmed electrical stimulation was performed using a standard protocol with 120

349 ms and 100 ms drive trains and single extrastimuli to measure function of the AV node and the

350 conduction properties of atrial and ventricular tissue. The Wenckebach cycle length was

351 measured by progressively faster atrial pacing rates. Retrograde (VA) conduction cycle length

352 was measured by progressively slower ventricular pacing rates. Sinus node function was

353 determined by measuring the sinus node recovery time (SNRT) following 30 seconds of pacing

354 at three cycle lengths (120, 100 and 80 ms). SNRT was divided by the basic cycle length to

355 adjust for the intrinsic heart rate.

Ambulatory ECG telemetry

Continuous ambulatory ECG telemetry was performed by implanting an ETA-F10 transmitter (Data Sciences International) during general anaesthesia with isoflurane. The transmitter was implanted in the abdomen and the leads were tunneled subcutaneously to the upper right and lower left chest resulting in a lead II position. Telemetry data was recorded continuously via a receiver placed under the mouse cage. Data analysis was performed using LabChart Pro software (AD Instruments).

Surface ECG

Mice were anesthetized as described above and surface ECG was recorded using subcutaneous electrodes connected to the Animal Bio amplifier and PowerLab station (AD Instruments). The ECG channel was filtered between 0.3 and 1000 Hz and analyzed using LabChart Pro software. Atropine (1 mg/kg), epinephrine (2 mg/kg) or isoproterenol (20 mg/kg) were administered intravenously, and changes were examined before and after injection.

Optogenetics

Two days after tamoxifen treatment, $Cx_3cr1^{wt/CreER}$ (control) and $Cx_3cr1^{wt/CreER}$ $ChR2^{wt/fl}$ (Cx_3cr1 $ChR2$) mice were euthanized and the hearts were perfused in a custom-built, horizontal perfusion bath in Langendorff mode with oxygenized Krebs-Henseleit solution containing (in mM): 118 NaCl, 4.7 KCl, 1.2 $MgSO_4$, 1.55 $CaCl_2$, 24.9 $NaHCO_3$, 1.2 KH_2PO_4, 11.1 Dextrose, pH 7.4 (all Sigma). Recording and electrical pacing electrodes were connected to the heart, and the endocardial surface overlying the AV node was exposed by carefully opening the right atrial free wall above the AV groove. Mean perfusion pressure was maintained at between 60-80 mmHg

377 throughout the experiment and adequacy of the preparation was determined by robust return of

378 sinus rhythm in the perfused heart and visual evidence of vigorous contraction. The location of

379 the AV node was identified grossly under a dissecting microscope. The Wenckebach cycle

380 length was first determined without illumination by determining the electrical stimulation atrial

381 pacing rate at which progressive PR interval prolongation occurred, culminating in a non-

382 conducted atrial impulse due to AV block. The heart was subsequently electrically paced at the

383 determined Wenckebach cycle length and the AV node was subjected to alternating 10-second

384 cycles with and without continuous AV node illumination. Continuous illumination of the

385 exposed AV node was performed using a 400-µm core fiber optic cannula coupled to a 470-nm

386 LED (ThorLabs) at light intensities of 55.7 mW/mm^2. The recorded ECG tracings were analyzed

387 using LabChart Pro software. The average Wenckebach ratio, which is defined as the number of

388 conducted atrial stimuli between two consecutive non-conducted impulses and is a sensitive

389 measure of relative degree of AV block, was determined for each light off and on cycle.

390 **Tissue processing**

391 Peripheral blood for flow cytometric analysis was collected by retro-orbital bleeding using

392 heparinized capillary tubes (BD Diagnostics) and red blood cells were lysed with 1x red blood

393 cell lysis buffer (BioLegend). To determine electrolyte levels, blood was collected by cardiac

394 puncture and electrolytes were measured on serum with EasyLyte PLUS analyzer (Medica). For

395 organ harvest, mice were perfused through the LV with 10 mL of ice-cold PBS. Hearts were

396 excised and processed as whole or subjected to AV node microdissection as described

397 previously[37]. Briefly, the triangle of Koch, which contains the AV node, was excised by using

398 the following landmarks: ostium of the coronary sinus, tendon of Todaro and septal leaflet of the

399 tricuspid valve. The presence of the AV node was confirmed with HCN4 and

400 acetylcholinesterase staining (see below). After harvest, cardiac tissues were minced into small

401 pieces and subjected to enzymatic digestion with 450 U/mL collagenase I, 125 U/mL collagenase

402 XI, 60 U/mL DNase I, and 60 U/mL hyaluronidase (all Sigma) for 20 minutes (microdissected

403 AV node) or 1 hour (whole heart) at 37°C under agitation. Tissues were then triturated and cells

404 filtered through a 40-µm nylon mesh (BD Falcon), washed and centrifuged to obtain single-cell

405 suspensions. Peritoneal cells were recovered by lavage with 5 mL of ice-cold PBS supplemented

406 with 3% fetal bovine serum and 2 mM EDTA.

Flow cytometry

407

408 Isolated cells were first stained at 4°C in FACS buffer (PBS supplemented with 0.5% bovine

409 serum albumin) with mouse hematopoietic lineage markers including phycoerythrin (PE) anti-

410 mouse antibodies directed against B220 (BioLegend, clone RA3-6B2, 1:600), CD49b

411 (BioLegend, clone DX5, 1:1200), CD90.2 (BioLegend, clone 53-2.1, 1:3000), Ly6G

412 (BioLegend, clone 1A8, 1:600), NK1.1 (BioLegend, clone PK136, 1:600) and Ter119

413 (BioLegend, clone TER-119, 1:600). This was followed by a second staining for CX_3CR1

414 (BioLegend, clone SA011F11, 1:600), CD11b (BioLegend, clone M1/70, 1:600), CD11c

415 (BioLegend, clone N418, 1:600), CD45 (BD Biosciences, clone 30-F11, 1:600 or BioLegend,

416 clone 104, 1:600), CD64 (BioLegend, clone X54-5/7.1, 1:600), CD103 (BioLegend, clone 2E7,

417 1:600), CD115 (eBioscience, clone AFS98, 1:600), F4/80 (Biolegend, clone BM8, 1:600) and/or

418 Ly6C (BioLegend, clone HK1.4, 1:600 or BD Bioscience, clone AL-21, 1:600). Monocytes were

419 identified as $(B220/CD49b/CD90.2/Ly6G/NK1.1/Ter119)^{low}$ $CD11b^{high}$ $CD115^{high}$ $Ly6C^{low/high}$.

420 Cardiac macrophages were identified as $(B220/CD49b/CD90.2/Ly6G/NK1.1/Ter119)^{low}$

421 $(CD45/CD11b)^{high}$ $Ly6C^{low/int}$ $F4/80^{high}$. Data were acquired on an LSRII (BD Biosciences) and

422 analyzed with FlowJo software (Tree Star).

Cell sorting

To isolate peritoneal macrophages, depletion of undesired cells including lymphocytes was performed using MACS depletion columns according to the manufacturer's instructions (Miltenyi). Briefly, single cell suspensions after peritoneal lavage were stained using a cocktail of PE-conjugated antibodies directed against B220, CD49b, CD90.2, NK1.1 and Ter119, followed by incubation with anti-PE microbeads. The enrichment of peritoneal macrophages was evaluated by flow cytometry. To purify macrophages from AV node tissue, digested samples were stained with hematopoietic lineage markers, CD11b, CD45, F4/80 and Ly6C, and macrophages were FACS-sorted using a FACSAria II cell sorter (BD Biosystems). DAPI was used as a cell viability marker. To isolate cardiac macrophages from whole heart, digested tissue samples were first enriched for CD11b$^+$ cells using CD11b microbeads and MACS columns according to the manufacturer's instructions (Miltenyi). Next, cells were stained with hematopoietic lineage markers, CD45, F4/80 and Ly6C, and FACS-sorted using a FACSAria II cell sorter.

Scrape-loading and dye-transfer assay

C57BL/6 mice were intravenously injected with 4 μg of CX$_3$CR1-APC antibody (BioLegend, clone SA011F11) to label tissue-resident macrophages. After 30 minutes of *in vivo* labeling, mice were perfused through the LV with 10 mL of oxygenated and prewarmed Tyrode's solution containing (in mM): 140 NaCl, 5.4 KCl, 1.8 CaCl$_2$, 1 MgCl$_2$, 10 glucose and 10 HEPES, pH 7.4 with NaOH (all Sigma). The AV node was microdissected in oxygenated and prewarmed Tyrode's solution as described above, and incubated in Tyrode's solution containing 2.5 mg/mL Lucifer yellow (Molecular Probes) for 2 minutes. The tissue was then washed with Tyrode's

445   solution for 5 minutes. After washing, the AV node was mounted between two long coverslips

446   and imaged using an Olympus IV100 microscope and z-stack images acquired at 1-2 μm steps

447   were processed with ImageJ software (NIH). Control tissue was handled as above, but with

448   omission of Lucifer yellow, and revealed negligible autofluorescence.

449   **Isolation and culture of neonatal mouse cardiomyocytes**

450   Neonatal mouse cardiomyocytes were isolated by use of enzymatic dissociation. One- to 2-day-

451   old pups were sacrificed, the hearts removed and the ventricles harvested. The tissue was

452   dissociated in HBSS containing 0.1% trypsin (Sigma) overnight at 4°C under agitation, followed

453   by three consecutive digestion steps in HBSS containing 335 U/mL collagenase II (Worthington

454   Biochemical Corporation) for 2 minutes at 37°C with gentle agitation. The digest was filtered

455   through a 40-μm nylon mesh, washed and resuspended in mouse culture medium which

456   consisted of DMEM supplemented with 14% FBS and 2% penicillin/streptomycin. Cell

457   suspensions were preplated into 100-mm cell tissue culture dishes and incubated at 37°C for 45

458   minutes to allow preferential attachment of non-myocyte cell populations and enrichment of the

459   cardiomyocyte population. Cardiac cells remaining in suspension were collected and seeded at a

460   density of $0.5\text{-}1\text{x}10^5$ cells/cm^2 on fibronectin-coated 8-mm cover slips (Warner Instruments) pre-

461   seeded with $5\text{x}10^4$ FACS-purified GFP$^+$ cardiac macrophages. Medium exchanges were

462   performed on the first day after seeding and every other day thereafter with mouse culture

463   medium supplemented with 1 μM cytosine β-D-arabinofuranoside hydrochloride (Sigma).

464   Experiments were performed on day 3.

465

Whole-cell patch clamp

Membrane potentials were recorded with whole-cell patch clamp technique in tight-seal current-clamp mode at 37°C. Borosilicate-glass electrodes filled with pipette solution had 4 to 6 MΩ tip resistance, and were connected with an Axopatch 200B amplifier and a Digidata 1440A A/D converter. Data were analyzed with Clampfit 9.2 (Molecular Devices). The bath solution contained (in mM): 136 NaCl, 5.4 KCl, 1 MgCl$_2$, 1.8 CaCl$_2$, 0.33 NaH$_2$PO$_4$, 5 HEPES, 10 Dextrose, pH 7.4 with NaOH, and the pipette solution contained (in mM): 110 K-aspartate, 20 KCl, 1 MgCl$_2$, 5 MgATP, 0.1 GTP, 10 HEPES, 5 Na-Phosphocreatine, 0.05 EGTA, pH 7.3 with KOH (all Sigma). To identify the patched cell, the pipette was additionally loaded with 0.2 mg/mL TexasRed$^+$ dextran (Molecular Probes, MW 3000). To block Cx43-mediated gap junction communication, 200 µM of the Cx43-mimetic peptide Gap26 (Alpha Diagnostics) was added to the batch solution during patch clamp recording.

Voltage dye imaging

Cardiomyocyte-macrophage co-cultures were loaded with 4 µM of ANNINE-6plus (Sensitive Farbstoffe GbR) for 5 minutes in Tyrode's solution. After washing, cover slips were transferred to Tyrode's solution containing 20 µM of blebbistatin (Sigma) to uncouple the excitation-contraction process in cardiomyocytes. To optically detect action potentials, line scans were obtained from the surface membranes of cardiomyocytes and attached macrophages using an Olympus IV100 microscope. The acquired line-scans were filtered with a collaborative filter to increase the signal-to-noise ratio and analyzed in Matlab (Mathworks) as previously described[38]. In detail, the average signal intensity of each successive line in the line-scan image corresponding to the membrane of the cell of interest was calculated to obtain the time course of

488   the averaged fluorescence [F(t)]. The time course of normalized fractional fluorescence changes

489   [$\Delta F/F_0(t)$], where ΔF is $F(t) - F_0(t)$ and $F_0(t)$ is the baseline trace, was subsequently determined

490   for the cardiomocyte and attached macrophage.

491   **Histology**

492   *Immunofluorescence staining:* To eliminate blood contamination, hearts were perfused with 10

493   mL of ice-cold PBS. Hearts from *Cx3cr1 ChR2*, *Cx3cr1 Cx43$^{-/-}$*, *Csf1^{op}* and *Cd11b^{DTR}* mice were

494   embedded in OCT compound and flash-frozen in a 2-methylbutane bath on dry ice. Serial frozen

495   6- to 25-µm sections were prepared and acetylcholinesterase staining (MBL) was carried out to

496   identify the AV node. The selected sections were fixed with 10% formalin for 5 minutes, washed

497   and permeabilized with 0.1% Triton X-100 in PBS for 30 minutes. The tissue sections were then

498   blocked with 4% normal goat serum in PBS for 30 minutes at room temperature. After blocking,

499   sections were incubated with a rabbit anti-mouse HCN4 antibody (Alomone labs) overnight at

500   4°C, followed by a biotinylated goat anti-rabbit IgG antibody for 45 minutes and DyLight 649-

501   streptavidin (Vector Laboratories) for 30 minutes at room temperature. The sections from *Cx3cr1*

502   *ChR2* hearts were additionally incubated with a chicken anti-GFP antibody (Abcam) overnight at

503   4°C. Alexa Fluor 568 goat anti-chicken IgG antibody (Life Technologies) was used as a

504   secondary antibody. The sections from *Cx3cr1 Cx43$^{-/-}$* and *Csf1^{op}* hearts were additionally

505   incubated with a rat anti-mouse CD68 antibody (AbD Serotec, clone: FA11) for 2 hours at room

506   temperature. Alexa Fluor 568 goat anti-rat IgG antibody (Life Technologies) was used as a

507   secondary antibody. TUNEL staining was performed using DeadEnd Fluorometric TUNEL

508   system (Promega) according to the manufacturer's protocol and DAPI was applied for nuclear

509   counterstaining. Cover slips seeded with cardiomyocytes and GFP$^+$ FACS-purified cardiac

510   macrophages were fixed with 4% PFA for 10 minutes at room temperature. After washing, cells

511   were permeabilized with 0.1% Triton X-100 in PBS for 10 minutes at room temperature, washed

512   and blocked in blocking solution (PBS containing 10% goat serum, 0.1% Tween-20 and 0.3 M

513   glycine) for 1 hour at room temperature. Cells were then stained with rabbit anti-mouse Cx43

514   antibody (Sigma) in blocking solution for 1 hour at room temperature, followed by incubation

515   with Alexa Fluor 647 goat anti-rabbit IgG secondary antibody (Life Technologies) for 1 hour at

516   room temperature. After washing, cells were stained with Alexa Fluor 568 rabbit anti-Desmin

517   antibody (Abcam) and DAPI was applied for nuclear counterstaining. All images were captured

518   using an Olympus FV1000 or a Nikon 80i fluorescence microscope and processed with ImageJ

519   software.

520   *Whole-mount immunofluorescence staining:* AV nodes from $Cx_3cr1^{GFP/+}$ mice were harvested as

521   described above and fixed using periodate-lysine-paraformaldehyde (PLP) in a 96-well plate for

522   1 hour at room temperature. Tissues were washed in 1% Triton X-100 diluted in PBS, and

523   blocked and permeabilized in blocking solution (PBS containing 20% goat serum, 1% Triton X-

524   100 and 0.2% sodium azide) for 1 hour at room temperature. AV nodes were then stained with

525   chicken anti-GFP (Abcam), rabbit anti-mouse Cx43 (Sigma) and rat anti-mouse HCN4 (Abcam)

526   antibodies in blocking solution for 3 days at 4°C. After washing, samples were incubated with

527   Alexa Fluor 488 goat anti-chicken IgG, Alexa Fluor 568 goat anti-rabbit IgG and Alexa Fluor

528   647 goat anti-rat IgG secondary antibodies (Life Technologies) overnight at 4°C. AV nodes were

529   then optically cleared or mounted between two long coverslips and imaged using an Olympus

530   FV1000 microscope and z-stack images acquired at 0.1- to 2-μm steps were processed with

531   ImageJ software.

532   *Optical clearing:* Stained AV nodes were cleared using Rapiclear 1.49 (SunJin Lab) by

533   immersion in the clearing solution for 24 hours at room temperature. The cleared tissues were

534   then mounted on a custom-made sample holder and imaged using an Olympus FV1000

535   microscope. Acquired images were processed with Amira 3D software (FEI Software).

536   *Immunohistochemistry:* Human AV node samples were stained with Masson's trichrome to

537   identify the cardiac conduction tissue. To identify human cardiac macrophages, the paraffin-

538   embedded tissue was first deparaffinized and antigen retrieval was performed using sodium

539   citrate, pH 6.0 (BD Biosciences). In order to block endogenous peroxidase activity, the tissue

540   sections were incubated in 1% H_2O_2 diluted in dH_2O for 10 minutes and rinsed in dH_2O and

541   PBS. The sections were then blocked with 4% horse serum in PBS for 30 minutes at room

542   temperature and incubated with a monoclonal mouse anti-human CD68 antibody (Dako, clone:

543   KP1) overnight at 4°C. A biotinylated horse anti-mouse IgG antibody (Vector Laboratories) was

544   applied for 30 minutes at room temperature. For color development, the VECTA STAIN ABC

545   kit (Vector Laboratories) and AEC substrate (Dako) were used. All the slides were

546   counterstained with Harris hematoxylin and scanned with NanoZoomer 2.0-RS (Hamamatsu).

547   Sections were analyzed at 20x magnification using iVision (BioVision Technologies).

548   *Electron microscopy:* Hearts from $Cx_3cr1^{GFP/+}$ mice were fixed using PLP solution and frozen

549   50-μm sections were incubated in 0.3% H_2O_2 diluted in PBS for 10 minutes, followed by

550   incubation with PBS containing 1% BSA and 0.05% saponin for 1 hour at room temperature. A

551   rabbit anti-GFP antibody (Life Technologies) was applied to the sections and incubated

552   overnight at 4°C. The tissue sections were washed and incubated with a biotinylated goat anti-

553   rabbit IgG antibody for 2 hours at room temperature. After washing, sections were incubated

554   with Vecta Stain ABC reagent for 30 minutes at room temperature, washed and then fixed with

555   PBS containing 1% glutaraldehyde and 5% sucrose for 30 minutes at room temperature. For

556   color development, diaminobenzidine solution was applied followed by 1% H_2O_2 in dH_2O. The

557   sections were washed and incubated with 1% osmium tetroxide in 0.1 M sodium cacodylate

558   buffer on ice for 30 minutes. Prior to embedding, sections were dehydrated and allowed to pre-

559   infiltrate in a 1:1 mix of Eponate resin and propylene oxide overnight at room temperature with

560   gentle agitation. Sections were then infiltrated with fresh 100% Eponate resin and polymerized

561   for 1-2 days at 60°C. Polymerized sections were trimmed and oriented such that the targeted AV

562   node region would lie at the sectioning face. Thin sections were cut using a Leica EM UC7

563   ultramicrotome, collected onto formvar-coated grids, stained with uranyl acetate and Reynold's

564   lead citrate and examined in a JEOL JEM 1011 transmission electron microscope at 80 kV.

565   Images were collected using an AMT digital imaging system (Advanced Microscopy

566   Techniques).

567   **YFP target-to-background ratio (TBR) measurement**

568   *$Cx_3cr1^{wt/wt}$* and *$Cx_3cr1^{wt/CreER}$* mice were intravenously injected with 4 µg of CX$_3$CR1-PE

569   (BioLegend, clone SA011F11) and Sca1-APC (BioLegend, clone E13-161.7) antibodies to label

570   tissue-resident macrophages and endothelial cells, respectively. After 30 minutes of *in vivo*

571   labeling, mice were perfused through the LV with 10 mL of ice-cold PBS. Hearts were then

572   mounted between two long coverslips and imaged using an Olympus IV100 microscope. *Z*-stack

573   images acquired at 1-µm steps were analyzed in Matlab with custom developed functions. Semi-

574   automatic thresholding-based algorithms were used for TBR measurements. A BM3D filter

575   method was implemented for noise reduction to increase the overall signal-to-noise ratio.

576

Western Blot

Total protein was extracted from heart tissue in RIPA lysis buffer (Pierce) supplemented with protease/phosphatase inhibitor cocktail (Cell Signaling). Protein concentration was measured using BCA assay (Pierce). Lysates of 3 µg were then subjected to electrophoresis using NuPAGE Novex Gel system (Life Technologies) and were blotted to nitrocellulose membrane using iBlot Gel Transfer system (Life Technologies) according to manufacturer's instructions. Anti-mouse Cx43 antibody (Sigma), anti-mouse GAPDH antibody (R&D Systems) and HRP-coupled secondary antibodies (Pierce) were used. Signals were visualized with chemiluminescent substrate (Pierce) and densitometric analysis was performed with ImageJ.

PCR confirmation of the deletion of the Cx43 allele

Genomic DNA from FACS-purified cardiac macrophages was isolated with DNeasy Blood & Tissue kit (Qiagen) and used in PCR with two pairs of *Cx43*-specific primers: 5'-CTTTGACTCTGATTACAGAGCTTAA-3' and 5'-GTCTCACTGTTACTTAACAGCTTGA-3' for detecting $Cx43^{fl}$ or $Cx43^{wt}$ alleles, and 5'-GCTACTTCTTGCTTTGACTCTGATTA-3' and 5'-GCTCACTTGATAGTCCACTCTAAGC-3' for detecting the *Cx43* allele lacking the floxed fragment. To normalize the amount of input DNA, specific primers to the Cx_3cr1^{wt} gene were used: 5'-GTCTTCACGTTCGGTCTGGT-3' and 5'-CCCAGACACTCGTTGTCCTT-3'.

qPCR

Total RNA from whole AV node tissue was extracted using the RNeasy Micro kit (Qiagen) or from FACS-purified cells using the Arcturus PicoPure RNA isolation kit (Applied Biosystems) according to the manufacturer's protocol. First-strand cDNA was synthesized using the High-

598   Capacity RNA-to-cDNA kit (Applied Biosystems) and pre-amplified using the TaqMan PreAmp

599   Master Mix kit (Applied Biosystems) according to the manufacturer's instructions. TaqMan gene

600   expression assays (Applied Biosystems) were used to quantify target genes. The relative changes

601   were normalized to *Gapdh* mRNA using the $2^{-\Delta\Delta CT}$ method.

602   **Bulk RNA-seq**

603   Total RNA from whole AV node tissue was extracted using the RNeasy Micro kit (Qiagen)

604   according to the manufacturer's protocol. The RNA quality was assessed with the RNA 6000

605   Pico assay kit using the Agilent Bioanalyzer. Sequencing-ready cDNA libraries were prepared

606   using the NEBNext Ultra RNA Directional Library Prep kit for Illumina (New England BioLabs)

607   following the manufacturer's protocol. Bioanalyzer traces were used to confirm library size

608   distribution. The libraries were quantified by qPCR using KAPA Library Quantification kit

609   (Kapa Biosystems) and then sequenced as single-end 50 base reads on a Illumina HiSeq 2000 in

610   high-output mode.

611   **Single-cell RNA-seq**

612   AV node macrophages were FACS-purified from whole AV node tissue as described above.

613   Single macrophages were then captured using the Fluidigm C1 microfluidic chip designed for 5-

614   to 10-µm cells according to the manufacturer's protocol. A concentration of 1.8×10^5 cells per mL

615   was used for chip loading. After cell capture, chips were examined visually to identify empty

616   chambers, which were excluded from later analysis. Cell lysis and cDNA synthesis were

617   performed on-chip with Clontech SMARTer Ultra Low RNA kit for the Fluidigm C1 system.

618   Amplified cDNA was validated and quantified on an Agilent Bioanalyzer with the High

619   Sensitivity DNA chip. Illumina libraries were then constructed in 96-well plates using the

620   Illumina Nextera XT DNA Sample Preparation kit according to a modified protocol supplied by

621   Fluidigm. Constructed libraries were validated and quantified with the Agilent High Sensitivity

622   DNA chip, and subsequently normalized and pooled to equal concentrations. The pooled

623   libraries were quantified by qPCR and sequenced as single-end 50 base reads on a Illumina

624   HiSeq 2000 in high-output mode.

625   **RNA-seq and microarray data analysis**

626   *Bulk RNA-seq:* Transcriptome mapping was performed with STAR version 2.3.0[39] using the

627   Ensembl 67 release exon/splice-junction annotations. Approximately 65-78% of reads mapped

628   uniquely. Read counts for individual genes were calculated using the unstranded count feature in

629   HTSeq v.0.6.0[40]. Differential expression analysis was performed using the exactTest routine of

630   the edgeR R package[41] after normalizing read counts and including only those genes with counts

631   per million (cpm) > 1 for two or more replicates. Differentially expressed genes were then

632   defined as those genes with > 2-fold change in expression and false discovery rate (FDR) < 0.05.

633   Hierarchical clustering of differentially expressed genes was performed with the heatmap.2

634   function in the R gplots library. Gene Set Enrichment Analysis (GSEA) was performed as

635   described previously[42]. Input rankings were based on the sign of the fold change multiplied by

636   the inverse of the *P* value. Genes involved in cardiac conduction (gene ontology term

637   GO:0061337, 38 unique members) were downloaded from the QuickGO Browser

638   (http://www.ebi.ac.uk/QuickGO/).

639   *Single-cell RNA-seq:* Transcriptome mapping (73-87% reads were uniquely mapped) and counts

640   per gene calculations were performed in the same manner as with the bulk RNA-seq data. The 76

641   cells with the most reads (260K – 6.3M, median 2.1M) were selected for further analysis.

642 Expression thresholding for detected genes and calculation of overdispersion (i.e., higher than

643 expected variance) was performed with SCDE[43] using the clean.counts and pagoda.varnorm

644 routines, respectively, which resulted in 9,235 genes retained for further analysis. Hierarchical

645 clustering of the 200 most overdispersed genes was performed using the heatmap.2 function in

646 the R gplots library. To group cells into three co-expression categories based on *H2* and *Ccr2*

647 expression levels, we performed spectral clustering on their joint distribution based on log2(cpm)

648 values (specc command in the factoextra R library). Then, the two clusters with lowest average

649 *H2* expression were joined to form a larger cluster shown in orange in Extended Data Fig. 2a.

650 *Microarray:* Raw microarray data from[9] were downloaded from ArrayExpress

651 (www.ebi.ac.uk/arrayexpress), accession number E-MEXP-3347, and normalized using the

652 robust multi-array average[44]. GSEA was performed using standard parameters (gene set

653 permutation, signal-to-noise ratio as a ranking metric).

Computational modeling

655 Macrophages were modeled as unexcitable cells based on a fibroblast model[45]. The macrophage

656 model comprises an inwardly rectifying potassium current and an unspecific background current.

657 Supplementary Table 1 shows the constants of the resulting model. Potassium concentrations

658 were set to match experimental conditions. The remaining parameters C_m, G_b, and G_{Kir} were

659 fitted to experimental whole-cell patch clamp data. The membrane capacitance of the model, C_m,

660 was set to the mean of the measured macrophage membrane capacitances ($n = 18$). The

661 conductance of the unspecific background current, G_b, was set to the inverse of the mean of

662 measured membrane resistances ($n = 9$). Finally, the maximal conductance of the potassium

663 channel, G_{Kir}, was adapted such that the resulting resting membrane potential matched the

30

664 measurements ($n = 20$). The resulting resting membrane potential also served as initial value for

665 the membrane potential V_m of the model. A mathematical model of a rabbit AV bundle

666 cardiomyocyte[46] was adapted to mouse cells to be able to estimate the effects of macrophage

667 coupling to an AV bundle cardiomyocyte. The rabbit model was modified such that the action

668 potential duration (APD_{90}) was reduced from 48 ms to 30 ms, a physiological value for mouse

669 atrial cardiomyocytes[47]. For this purpose, we introduced two scaling factors for the time

670 constants of gating variables that correspond to the currents $I_{Ca,L}$, and I_{to}. Namely, in the altered

671 model it is $\tau_* = s_* \overline{\tau_*}$ for $* \in \{d, r, p_i\}$ where $\overline{\tau_*}$ is the corresponding original value from the

672 unaltered model. The resulting scaling factors of the modified model were $s_d = 0.5182$ and $s_r = $

673 7.0239.

674 **Statistics**

675 All statistical analyses were conducted with GraphPad Prism software (GraphPad Software) and

676 data are expressed as mean ± standard error (s.e.m.). All n numbers represent biological repeats

677 unless indicated otherwise. The data was tested for normality using the D'Agostino-Pearson

678 normality test and for equal variance. Statistical significance was assessed by the two-sided

679 Student's t-test for normally distributed data. If normal distribution or equal variance

680 assumptions were not valid, statistical significance was evaluated using the two-sided Mann-

681 Whitney test and the two-sided Wilcoxon rank-sum test. For multiple comparisons,

682 nonparametric Kruskal-Wallis tests followed by Dunn's posttest were performed. Statistical

683 significancy of contingency tables was assessed with a Fisher's exact test. The Mantel-Cox test

684 was used to compare onset of AV block in DT-treated mice. P values of 0.05 or less were

685 considered to denote significance. Animal group sizes were as low as possible and empirically

686   chosen. No statistical methods were used to predetermine sample size and animals were

687   randomly assigned to treatment groups. Tested samples were assayed in a blinded fashion.

688

REFERENCES

1. Metchnikoff, É. *Leçons sur la Pathologie Comparée de l'Inflammation* (Masson, Paris, 1892).

2. Nguyen, K. D. *et al.* Alternatively activated macrophages produce catecholamines to sustain adaptive thermogenesis. *Nature* **480**, 104-108 (2011).

3. Theurl, I. *et al.* On-demand erythrocyte disposal and iron recycling requires transient macrophages in the liver. *Nat Med* **22**, 945-951 (2016).

4. Paolicelli, R. C. *et al.* Synaptic pruning by microglia is necessary for normal brain development. *Science* **333**, 1456-1458 (2011).

5. Davies, L. C., Jenkins, S. J., Allen, J. E. & Taylor, P. R. Tissue-resident macrophages. *Nat Immunol* **14**, 986-995 (2013).

6. Tawara, S. *Das Reizleitungssystem des Säugetierherzens: eine anatomisch-histologische Studie über das Atrioventrikularbündel und der Purkinjeschen Fäden* (Verlag von Gustav Fischer, Jena, 1906).

7. Billette, J. Atrioventricular nodal activation during periodic premature stimulation of the atrium. *Am J Physiol* **252**, H163-77 (1987).

8. Rubart, M. & Zipes, D. P. in *Braunwald's Heart Disease* (eds Libby, P., Bonow, R. O., Mann, D. L. & Zipes, D.) 909-921 (Suanders Elsevier, Philadelphia, 2008).

9. Pinto, A. R. *et al.* An abundant tissue macrophage population in the adult murine heart with a distinct alternatively-activated macrophage profile. *PLoS One* **7**, e36814 (2012).

10. Heidt, T. *et al.* Differential contribution of monocytes to heart macrophages in steady-state and after myocardial infarction. *Circ Res* **115**, 284-295 (2014).

11. Epelman, S. *et al.* Embryonic and adult-derived resident cardiac macrophages are maintained through distinct mechanisms at steady state and during inflammation. *Immunity*

713   **40**, 91-104 (2014).

714   12.   Swirski, F. K. & Nahrendorf, M. Leukocyte behavior in atherosclerosis, myocardial

715   infarction, and heart failure. *Science* **339**, 161-166 (2013).

716   13.   Biel, M., Wahl-Schott, C., Michalakis, S. & Zong, X. Hyperpolarization-activated cation

717   channels: from genes to function. *Physiol Rev* **89**, 847-885 (2009).

718   14.   Unger, V. M., Kumar, N. M., Gilula, N. B. & Yeager, M. Three-dimensional structure of a

719   recombinant gap junction membrane channel. *Science* **283**, 1176-1180 (1999).

720   15.   Oviedo-Orta, E. & Howard Evans, W. Gap junctions and connexin-mediated

721   communication in the immune system. *Biochim Biophys Acta* **1662**, 102-112 (2004).

722   16.   Shibata, Y. & Yamamoto, T. Gap junctions in the cardiac muscle cells of the lamprey. *Cell

723   Tissue Res* **178**, 477-482 (1977).

724   17.   Ongstad, E. & Kohl, P. Fibroblast-myocyte coupling in the heart: Potential relevance for

725   therapeutic interventions. *J Mol Cell Cardiol* **91**, 238-246 (2016).

726   18.   Neijssen, J., Pang, B. & Neefjes, J. Gap junction-mediated intercellular communication in

727   the immune system. *Prog Biophys Mol Biol* **94**, 207-218 (2007).

728   19.   Gautier, E. L. *et al.* Gene-expression profiles and transcriptional regulatory pathways that

729   underlie the identity and diversity of mouse tissue macrophages. *Nat Immunol* **13**, 1118-

730   1128 (2012).

731   20.   Park, D. S. & Fishman, G. I. The cardiac conduction system. *Circulation* **123**, 904-915

732   (2011).

733   21.   Rosas, M. *et al.* The transcription factor Gata6 links tissue macrophage phenotype and

734   proliferative renewal. *Science* **344**, 645-648 (2014).

735   22.   Nikolski, V. P., Jones, S. A., Lancaster, M. K., Boyett, M. R. & Efimov, I. R. Cx43 and

736   dual-pathway electrophysiology of the atrioventricular node and atrioventricular nodal

737   reentry. *Circ Res* **92**, 469-475 (2003).

738   23.   Hucker, W. J., McCain, M. L., Laughner, J. I., Iaizzo, P. A. & Efimov, I. R. Connexin 43

739   expression delineates two discrete pathways in the human atrioventricular junction. *Anat*

740   *Rec (Hoboken)* **291**, 204-215 (2008).

741   24.   Rohr, S. Role of gap junctions in the propagation of the cardiac action potential.

742   *Cardiovasc Res* **62**, 309-322 (2004).

743   25.   Nerbonne, J. M., Nichols, C. G., Schwarz, T. L. & Escande, D. Genetic manipulation of

744   cardiac K(+) channel function in mice: what have we learned, and where do we go from

745   here. *Circ Res* **89**, 944-956 (2001).

746   26.   Gallin, E. K. & Gallin, J. I. Interaction of chemotactic factors with human macrophages.

747   Induction of transmembrane potential changes. *J Cell Biol* **75**, 277-289 (1977).

748   27.   Gallin, E. K. & Livengood, D. R. Nonlinear current-voltage relationships in cultured

749   macrophages. *J Cell Biol* **85**, 160-165 (1980).

750   28.   Kohl, P. & Gourdie, R. G. Fibroblast-myocyte electrotonic coupling: does it occur in native

751   cardiac tissue. *J Mol Cell Cardiol* **70**, 37-46 (2014).

752   29.   Fenno, L., Yizhar, O. & Deisseroth, K. The development and application of optogenetics.

753   *Annu Rev Neurosci* **34**, 389-412 (2011).

754   30.   Nagel, G. *et al.* Channelrhodopsin-2, a directly light-gated cation-selective membrane

755   channel. *Proc Natl Acad Sci U S A* **100**, 13940-13945 (2003).

756   31.   Cecchini, M. G. *et al.* Role of colony stimulating factor-1 in the establishment and

757   regulation of tissue macrophages during postnatal development of the mouse. *Development*

758   **120**, 1357-1372 (1994).

759   32.   Nisbet, A. M. *et al.* Prolongation of atrio-ventricular node conduction in a rabbit model of

760   ischaemic cardiomyopathy: Role of fibrosis and connexin remodelling. *J Mol Cell Cardiol*

761   **94**, 54-64 (2016).

762   33.   Catterall, W. A. Voltage-gated calcium channels. *Cold Spring Harb Perspect Biol* **3**,

763   a003947 (2011).

764   34.   Zoob, M. & Smith, K. S. The Aetiology of complete heart-block. *Br Med J* **2**, 1149-1153

765   (1963).

766   35.   Sager, H. B. *et al.* Proliferation and Recruitment Contribute to Myocardial Macrophage

767   Expansion in Chronic Heart Failure. *Circ Res* **119**,

768   doi:10.1161/CIRCRESAHA.116.309001 (2016).

769   36.   Bunch, T. J., Hohnloser, S. H. & Gersh, B. J. Mechanisms of sudden cardiac death in

770   myocardial infarction survivors: insights from the randomized trials of implantable

771   cardioverter-defibrillators. *Circulation* **115**, 2451-2457 (2007).

772   37.   Moskowitz, I. P. *et al.* A molecular pathway including Id2, Tbx5, and Nkx2-5 required for

773   cardiac conduction system development. *Cell* **129**, 1365-1376 (2007).

774   38.   Bu, G., Adams, H., Berbari, E. J. & Rubart, M. Uniform action potential repolarization

775   within the sarcolemma of in situ ventricular cardiomyocytes. *Biophys J* **96**, 2532-2546

776   (2009).

777   39.   Dobin, A. *et al.* STAR: ultrafast universal RNA-seq aligner. *Bioinformatics* **29**, 15-21

778   (2013).

779   40.   Anders, S., Pyl, P. T. & Huber, W. HTSeq--a Python framework to work with high-

780   throughput sequencing data. *Bioinformatics* **31**, 166-169 (2015).

781   41.   Robinson, M. D., McCarthy, D. J. & Smyth, G. K. edgeR: a Bioconductor package for

782	differential expression analysis of digital gene expression data. *Bioinformatics* **26**, 139-140

783	(2010).

784	42.	Mootha, V. K. *et al.* PGC-1alpha-responsive genes involved in oxidative phosphorylation

785	are coordinately downregulated in human diabetes. *Nat Genet* **34**, 267-273 (2003).

786	43.	Kharchenko, P. V., Silberstein, L. & Scadden, D. T. Bayesian approach to single-cell

787	differential expression analysis. *Nat Methods* **11**, 740-742 (2014).

788	44.	Irizarry, R. A. *et al.* Exploration, normalization, and summaries of high density

789	oligonucleotide array probe level data. *Biostatistics* **4**, 249-264 (2003).

790	45.	Sachse, F. B., Moreno, A. P. & Abildskov, J. A. Electrophysiological modeling of

791	fibroblasts and their interaction with myocytes. *Ann Biomed Eng* **36**, 41-56 (2008).

792	46.	Inada, S., Hancox, J. C., Zhang, H. & Boyett, M. R. One-dimensional mathematical model

793	of the atrioventricular node including atrio-nodal, nodal, and nodal-his cells. *Biophys J* **97**,

794	2117-2127 (2009).

795	47.	Xu, H., Li, H. & Nerbonne, J. M. Elimination of the transient outward current and action

796	potential prolongation in mouse atrial myocytes expressing a dominant negative Kv4 alpha

797	subunit. *J Physiol* **519 Pt 1**, 11-21 (1999).

798

ACKNOWLEDGEMENTS

AUTHOR CONTRIBUTIONS

M.H., S.C., L.X., A.D.A and K.R.K. performed experiments, collected, analyzed and discussed data. A.H., W.J.H., E.M.W., G.S., G.C., Y.I., Y.S., H.B.S., K.J.L., D.E.C., N.D.S., L.M., K.N. and C.V. performed experiments and collected data. G.A.F. and R.N.M. provided human AV

821   node tissue. D.B., P.L., R.W., F.K.S., P.K., C.V., D.J.M. and P.T.E. conceived experiments and

822   discussed results and strategy. M.N. conceived, designed and directed the study. M.H. and M.N.

823   wrote the manuscript, which was revised and approved by all authors.

824

829
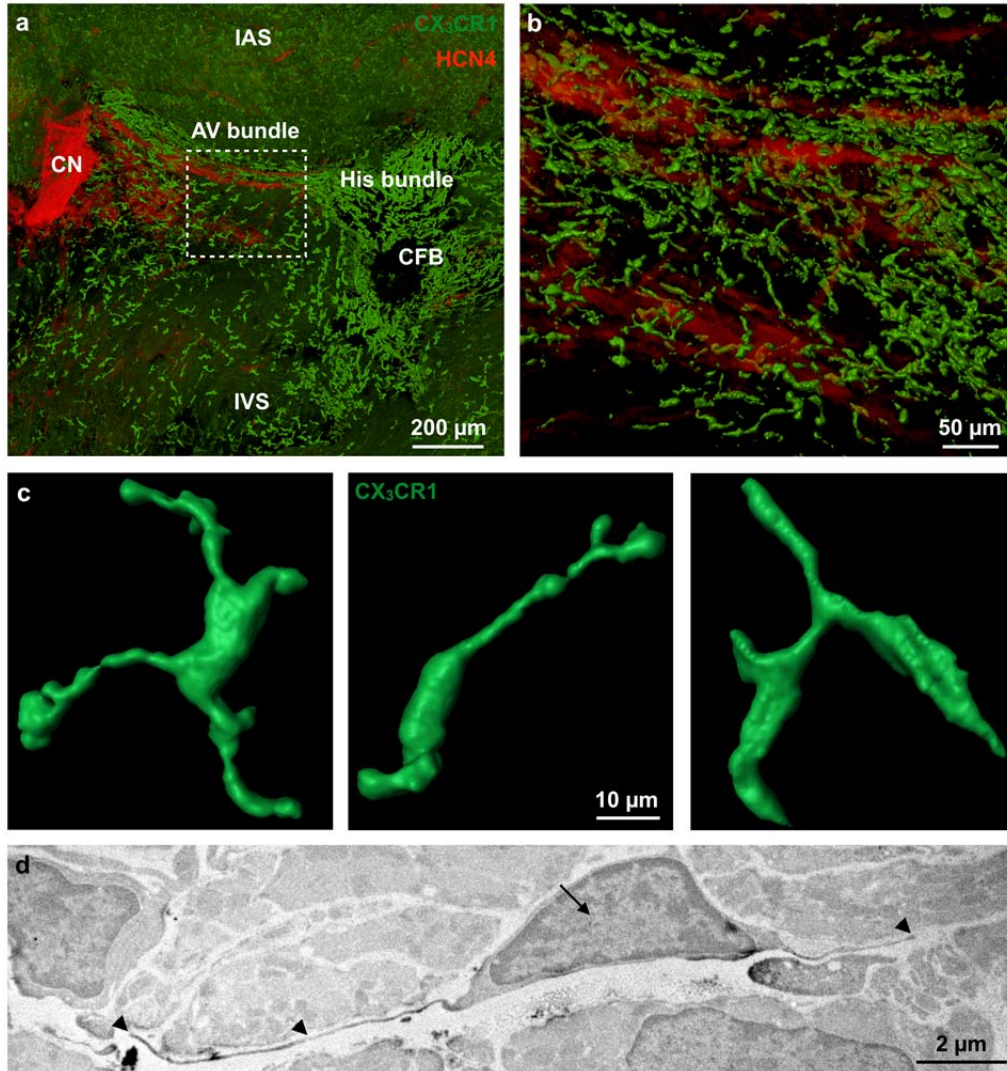
830

831

832 **Figure 1** | **Resident cardiac macrophages in the AV node. a,** Volumetric reconstruction of
833 confocal microscopy after optical clearing of the atrioventricular (AV) node in a $Cx_3cr1^{GFP/+}$
834 mouse stained with HCN4 (red). The node is orientated along the AV groove extending from the
835 compact node (CN) into the proximal His bundle. Dashed square indicates the lower nodal or
836 AV bundle. CFB, central fibrous body; IAS and IVS, interatrial and interventricular septum. **b,**
837 Higher magnification of dashed square in (a). **c,** 3D rendering of GFP[+] macrophages in the AV
838 bundle. **d,** Electron microscopy of a DAB[+] macrophage in AV node of $Cx_3cr1^{GFP/+}$ mouse
839 stained with a primary antibody for GFP. Arrow indicates nucleus, arrowheads indicate cellular
840 processes.

841

842
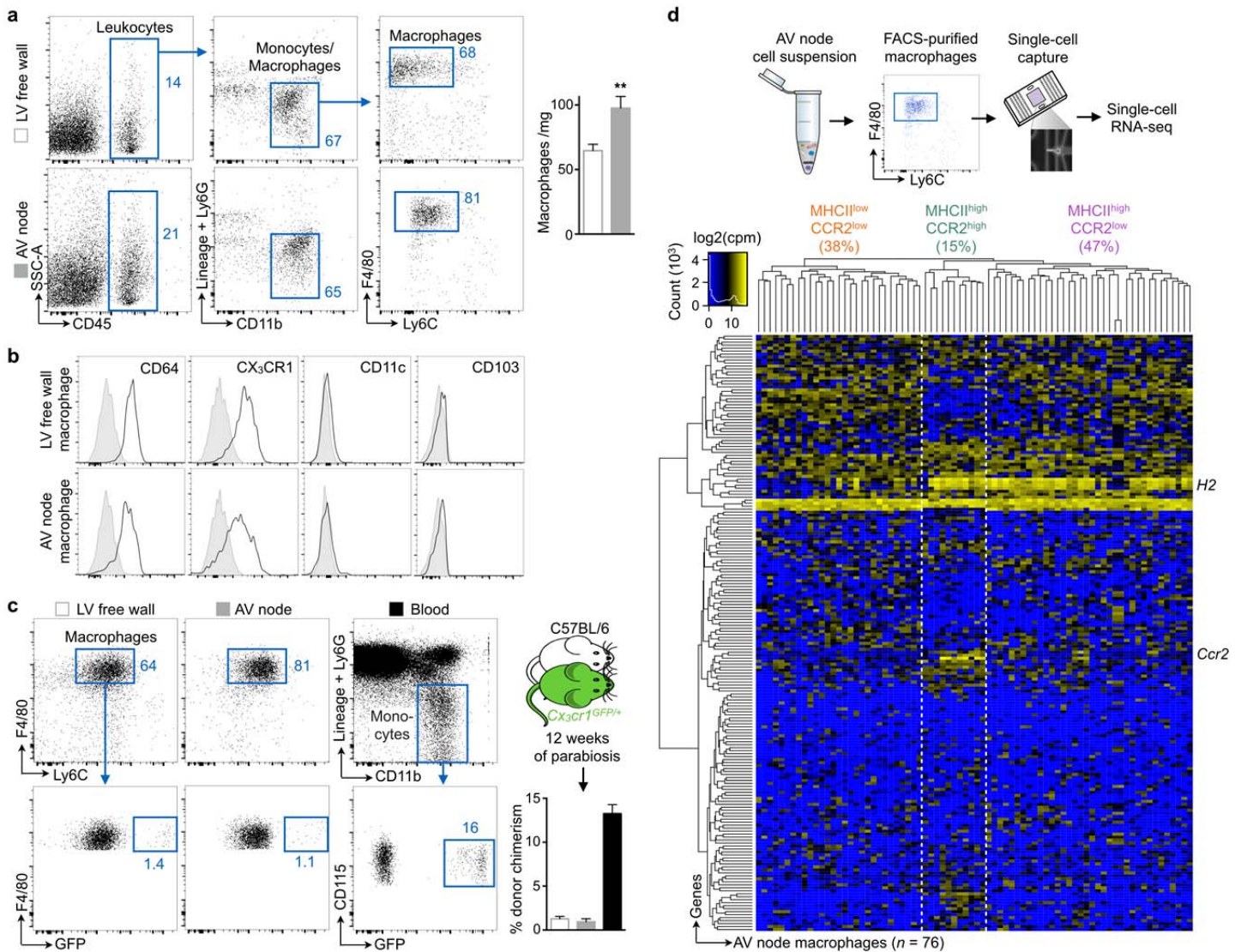
Figure 2 | **The AV node enriches for macrophages. a,** Flow cytometric macrophage
quantification in microdissected AV node and left ventricular (LV) free wall of C57BL/6 mice.
(Left) Representative flow cytometry plots; (right) number of macrophages per mg of heart
tissue. Data are mean ± s.e.m., n = 12 mice of 4 independent experiments, $^{**}P < 0.01$, Student's
t-test. **b,** Expression of CD64, CX$_3$CR1, CD11c and CD103 on AV node and LV free wall
macrophages. Representative histograms of 4 mice are shown. Gray, isotype control antibody. **c,**
Macrophage chimerism in the LV free wall and AV node and monocyte chimerism in the blood
of C57BL/6 mice that had been joined in parabiosis with $Cx_3cr1^{GFP/+}$ mice for 12 weeks (mean ±
s.e.m., n = 3 [AV node] and n = 7 [LV free wall and blood] of 2 independent experiments). **d,**
(Top) Workflow; (bottom) Heat map of expression levels (cpm, counts per million) among top
200 overdispersed genes from RNA-seq data of 76 AV node macrophages. Unsupervised
clustering reflects three macrophage subsets according to expression levels of *H2* and *Ccr2*
(orange, MHCII^{low}CCR2^{low}; green, MHCII^{high}CCR2^{high}; purple, MHCII^{high}CCR2^{low}).

856
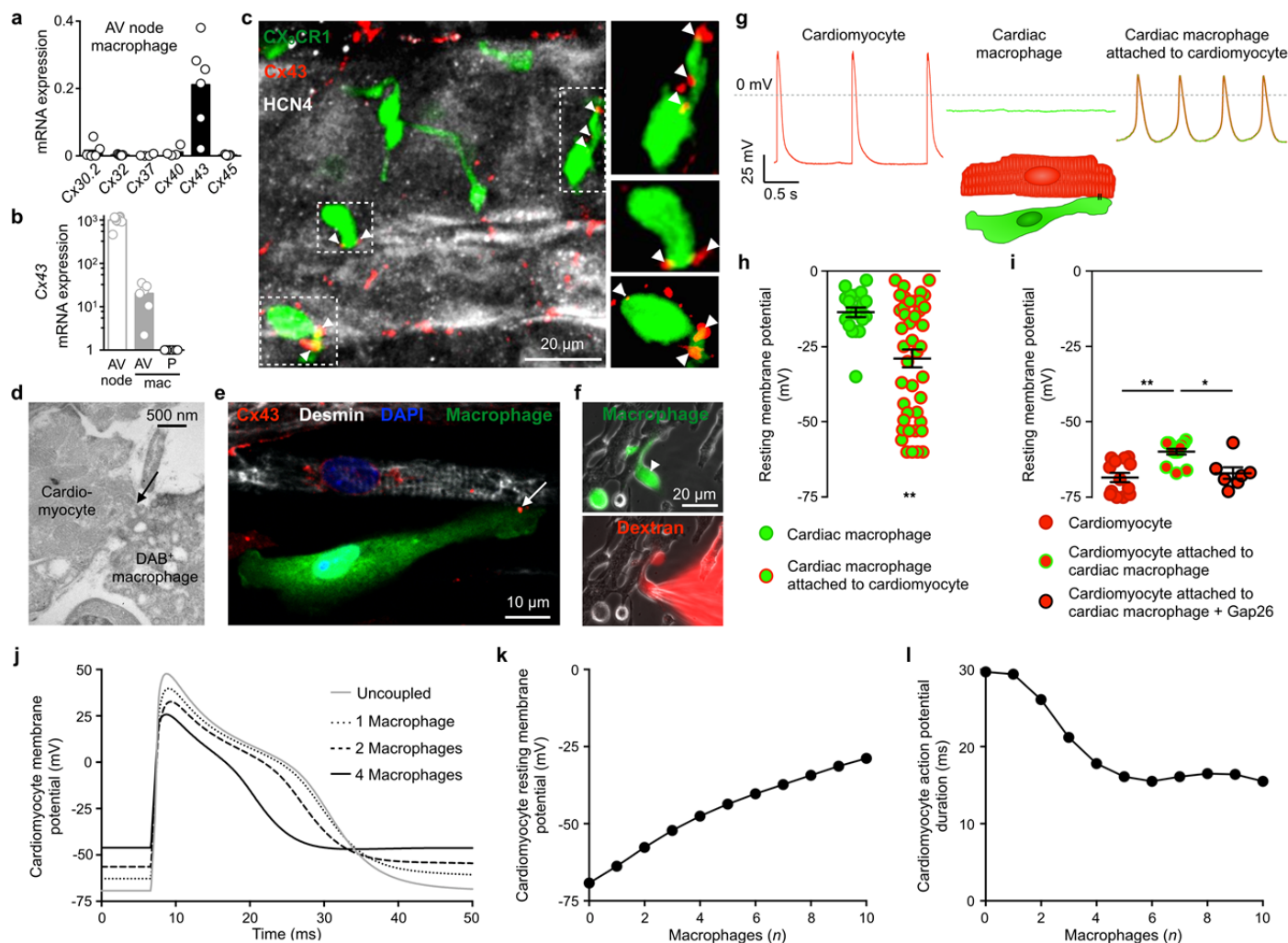
Figure 3 | AV node macrophages couple to conducting cardiomyocytes and alter their electrophysiological properties. a, Relative connexin (*Cx*) expression levels in FACS-purified AV node macrophages by qPCR (n = 4 to 6 of 2 independent experiments). **b,** *Cx43* levels by qPCR in whole AV node tissue and in macrophages FACS-sorted from AV node and peritoneum (P). n = 6 to 9 of 2 independent experiments; mac, macrophage. **c,** Whole-mount immunofluorescence microscopy of AV lower nodal area from a *Cx₃cr1*[GFP/+] mouse stained with Cx43 (red) and HCN4 (white). Arrowheads indicate Cx43 colocalization with GFP+ macrophages (green). **d,** Electron microscopy image of a direct membrane contact of a DAB+ macrophage and a cardiomyocyte in AV node tissue of *Cx₃cr1*[GFP/+] mouse stained for GFP. Arrow indicates membrane contact. **e,** Immunofluorescence image of a co-cultured desmin+ neonatal mouse cardiomyocyte (white) and GFP+ cardiac macrophage (green) stained with Cx43 (red, arrow), illustrating setup for patch clamp experiments (f-i). **f,** Immunofluorescence images of dextran diffusion during whole-cell patch clamp with a dextran-loaded pipette. (Top) Arrowhead indicates GFP+ cardiac macrophage (green); (bottom) TexasRed+ dextran (red) diffusion into macrophage. **g,** Spontaneous recordings and **h,** resting membrane potential of solitary cardiac macrophages (n = 20) and macrophages attached to cardiomyocytes (n = 43) by whole-cell patch clamp. Data are mean ± s.e.m. from 13 independent experiments, **P < 0.01,

nonparametric Mann-Whitney test. Rhythmic depolarization was observed in 10/43 macrophages attached to cardiomyocytes. **i,** Resting membrane potential of solitary cardiomyocytes ($n = 13$) and cardiomyocytes coupled to macrophages before ($n = 14$) and after ($n = 7$) addition of the Cx43 inhibitor Gap26. Data are mean ± s.e.m. from 3 independent experiments, [*]$P < 0.05$ and [**]$P < 0.01$, Kruskal-Wallis test followed by Dunn's posttest. **j,** Mathematical modeling of AV bundle cardiomyocyte membrane potential uncoupled or coupled to one, two or four cardiac macrophages at a junctional conductance of 1 nS. **k,** Computational modeling of resting membrane potential and **l,** action potential duration (APD_{90}) of an AV bundle cardiomyocyte coupled to an increasing number of cardiac macrophages.
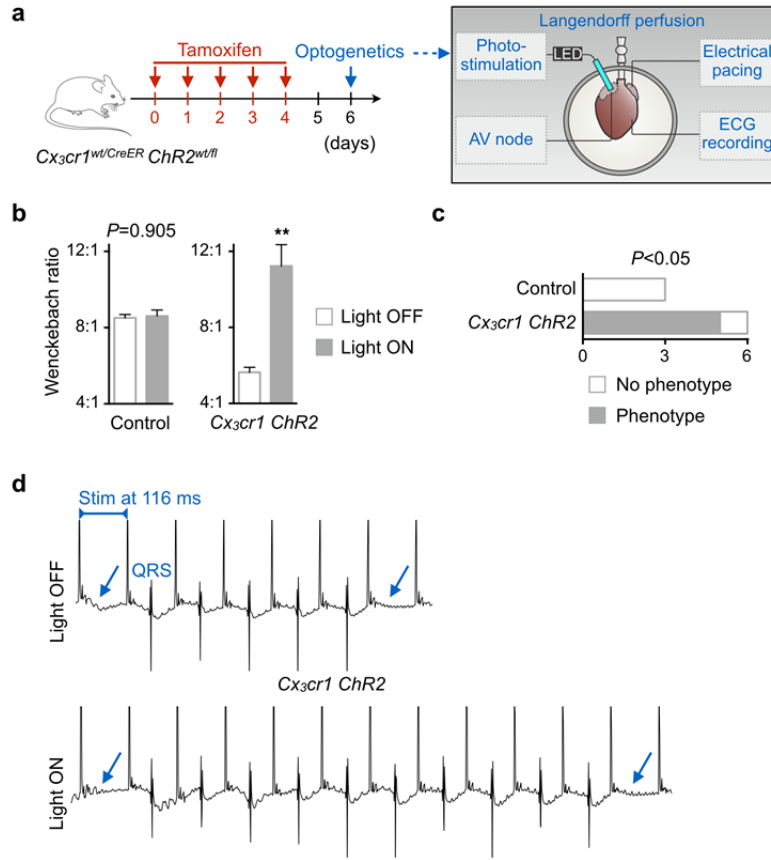
Figure 4 | **Optogenetics stimulation of AV node macrophages improves nodal conduction. a,**
Experimental outline. Hearts of $Cx_3cr1^{wt/CreER}$ (control) or tamoxifen-treated $Cx_3cr1^{wt/CreER}$
$ChR2^{wt/fl}$ (Cx_3cr1 $ChR2$) mice were perfused in a Langendorff setup. Recording and pacing
electrodes were connected to the heart and illumination with a fiber optic cannula was focused
on the AV node. **b,** Representative bar graphs of a control and Cx_3cr1 $ChR2$ heart showing the
Wenckebach ratio during light off and on cycles. Data are mean ± s.e.m., $^{**}P < 0.01$,
nonparametric Mann-Whitney test. **c,** Contingency graph of control ($n = 3$) and Cx_3cr1 $ChR2$ ($n = 6$) hearts indicating the presence of increased Wenckebach ratio phenotype during
photostimulation of the AV node. Fisher's exact test. **d,** Representative ECG recordings from a
Cx_3cr1 $ChR2$ heart illustrating the Wenckebach ratio during light off and on cycles. Arrows
indicate failure of conduction leading to missing QRS complexes. Stim, stimulation.
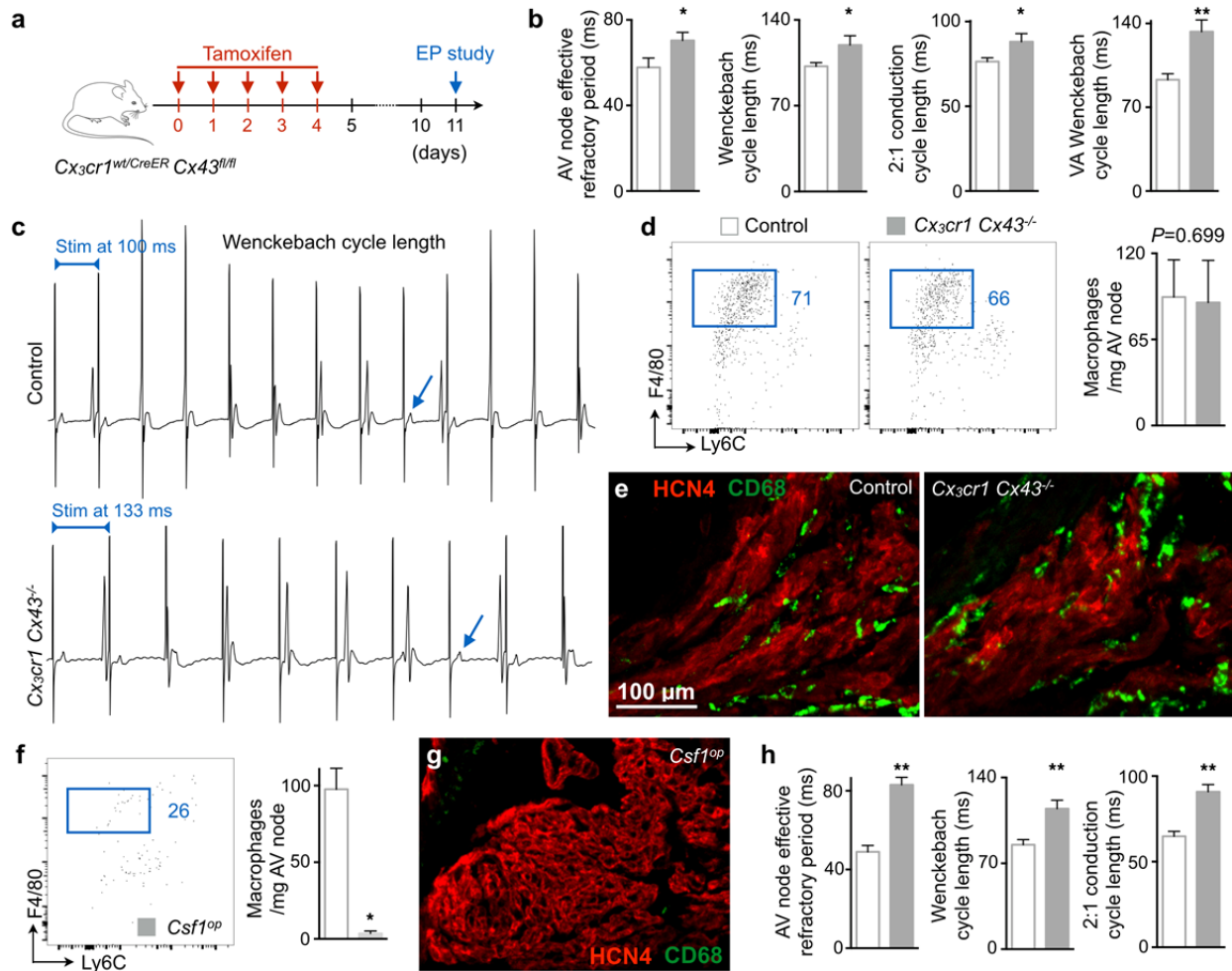
Figure 5 | **Cx43 deletion in macrophages and congenital lack of macrophages delay AV conduction. a,** Experimental outline of the electrophysiological (EP) study performed on mice lacking Cx43 in macrophages. **b,** AV node effective refractory period at 120 ms pacing frequency, and pacing cycle lengths at which Wenckebach conduction, 2:1 conduction and ventriculo-atrial (VA) Wenckebach conduction occurred in control (n = 5 to 9) and Cx_3cr1 $Cx43^{-/-}$ (n = 6 to 8) mice. Data are mean ± s.e.m., 2 independent experiments, $^*P < 0.05$ and $^{**}P < 0.01$, Student's t-test and nonparametric Mann-Whitney test. **c,** Surface ECG from control and Cx_3cr1 $Cx43^{-/-}$ mice illustrating the Wenckebach cycle length. Arrows indicate missing QRS complexes. Stim, stimulation. **d,** Flow cytometric quantification of AV node macrophages in control and Cx_3cr1 $Cx43^{-/-}$ mice. Data are mean ± s.e.m., n = 6 mice per group, nonparametric Mann-Whitney test. **e,** Immunofluorescence images of control and Cx_3cr1 $Cx43^{-/-}$ AV node stained for CD68 (green) and HCN4 (red). **f,** Quantification of AV node macrophages in control (n = 5) and $Csf1^{op}$ (n = 4) mice by flow cytometry. Data are mean ± s.e.m., 3 independent experiments, $^*P < 0.05$, nonparametric Mann-Whitney test. **g,** Immunofluorescence image of a $Csf1^{op}$ AV node stained for CD68 (green) and HCN4 (red). **h,** AV node effective refractory period at 120 ms pacing frequency, and pacing cycle lengths at which Wenckebach and 2:1 conduction occurred in control (n = 6) and $Csf1^{op}$ (n = 5) mice. Data are mean ± s.e.m., 3 independent experiments, $^{**}P < 0.01$, nonparametric Mann-Whitney test.

918

919
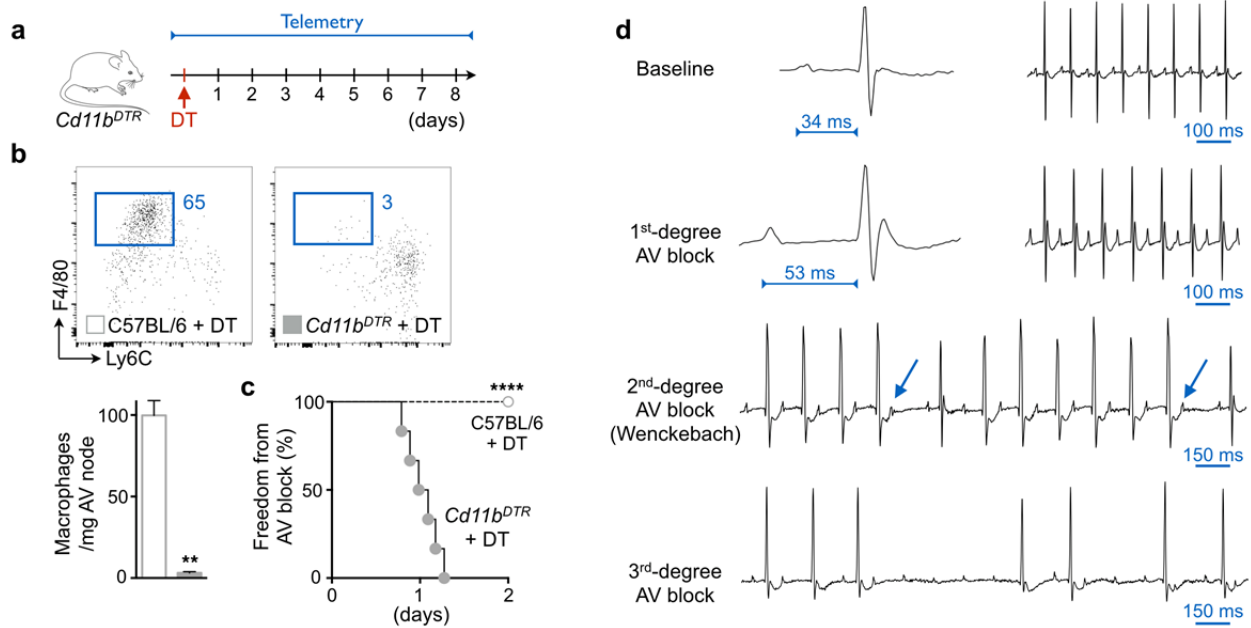
Figure 6 | **Macrophage ablation induces AV block. a,** Experimental outline. DT, diphtheria toxin. **b,** Flow cytometric quantification of AV node macrophages three days after intraperitoneal injection of DT into C57BL/6 and $Cd11b^{DTR}$ mice. Data are mean ± s.e.m., n = 6 mice per group, $^{**}P < 0.01$, nonparametric Mann-Whitney test. **c,** Onset of first degree AV block in $Cd11b^{DTR}$ (n = 6) and C57BL/6 (n = 10) animals after DT injection (2 independent experiments, $^{****}P <$ 0.0001, Mantel-Cox test). **d,** Telemetric ECG recordings before and after DT injection in $Cd11b^{DTR}$ mice. Arrows indicate non-conducted P waves in second degree AV block.